

Orbital magnetic moment and coercivity of SiO₂-coated FePt nanoparticles studied by x-ray magnetic circular dichroism

Y. Takahashi,^{1,*} T. Kadono,¹ V. R. Singh,¹ V. K. Verma,¹ K. Ishigami,² G. Shibata,¹ T. Harano,¹ A. Fujimori,^{1,3} Y. Takeda,³ T. Okane,³ Y. Saitoh,³ H. Yamagami,^{3,4} S. Yamamoto,⁵ and M. Takano⁵

¹*Department of Physics, University of Tokyo, Bunkyo-ku, Tokyo 113-0033, Japan*

²*Graduate School of Frontier Science, University of Tokyo, Bunkyo-ku, Tokyo 113-0033, Japan*

³*Quantum Beam Science Directorate, Japan Atomic Energy Agency, Sayo-cho, Sayo-gun, Hyogo 679-5148, Japan*

⁴*Department of Physics, Kyoto Sangyo University,*

Motoyama, Kamigamo, Kita-Ku, Kyoto 603-8555, Japan

⁵*Institute for Integrated Cell-Material Science (iCeMS), Kyoto University, Yoshida Ushinomiya-cho, Sakyo-ku, Kyoto 606-8501, Japan*

We have investigated the spin and orbital magnetic moments of Fe in FePt nanoparticles in the $L1_0$ -ordered phase coated with SiO₂ by x-ray absorption spectroscopy (XAS) and x-ray magnetic circular dichroism (XMCD) measurements at the Fe $L_{2,3}$ absorption edges. Using XMCD sum rules, we evaluated the ratio of the orbital magnetic moment (M_{orb}) to the spin magnetic moment (M_{spin}) of Fe to be $M_{\text{orb}}/M_{\text{spin}} = 0.08$. This $M_{\text{orb}}/M_{\text{spin}}$ value is comparable to the value (0.09) obtained for FePt nanoparticles prepared by gas phase condensation, and is larger than the values (~ 0.05) obtained for FePt thin films, indicating a high degree of $L1_0$ order. The hysteretic behavior of the FePt component of the magnetization was measured by XMCD. The magnetic coercivity (H_c) was found to be as large as 1.8 T at room temperature, ~ 3 times larger than the thin film value and ~ 50 times larger than that of the gas phase condensed nanoparticles. The hysteresis curve is well explained by the Stoner-Wohlfarth model for non-interacting single-domain nanoparticles with the H_c distributed from 1 T to 5 T.

PACS numbers: 78.20.Ls, 75.60.-d, 75.50.Bb, 75.75.Fk

The $L1_0$ -ordered alloy FePt has attracted great attention as a material to be used in high-density storage memory devices because FePt possesses a high magneto-crystalline anisotropy in bulk FePt and thin films¹⁻⁴. In order to increase the storage density of memory devices, FePt nanoparticles are promising materials. FePt nanoparticles prepared by the gas phase preparation method⁵ and the wet chemical preparation method⁶, however, have the fcc structure, in which magneto-crystalline anisotropy disappears. By annealing the nanoparticles at high temperatures, one can transform the structure from the fcc to $L1_0$, but then the nanoparticles are easily oxidized and are covered by surface oxides. The plasma treatments of FePt nanoparticles followed by *in situ* flight annealing have been performed to remove the oxidized surfaces^{7,8}, however, it has simultaneously reduced the magnetic coercivity (H_c) as small as 0.038 T⁸. In addition, high temperature annealing is difficult to implement in existing manufacturing process because it may lead to the coalescence of nanoparticles into larger particles⁹. Recently, in order to overcome such difficulties, FePt nanoparticles coated with SiO₂ were prepared and dispersed before annealing to achieve a high degree of $L1_0$ order^{6,9-13}. FePt nanoparticles prepared by this method have a H_c as large as 1.85 T at 300 K⁹, of the same order as the value of 3.0 T observed for $L1_0$ -FePt (001) particulate films¹⁴, and much larger than the bulk value of 0.16 T¹⁵, the thin film value of 0.55 T⁴, and the value of 0.75 T for microfabricated FePt (001) dots¹⁶.

In order to understand the origin of the large H_c and to further improve the properties of the SiO₂-coated FePt

nanoparticles, microscopic information about the magnetism such as the orbital magnetic moment is important. The chemical state of Fe can be easily distinguished by soft x-ray absorption spectroscopy (XAS), and the orbital and spin magnetic moments of transition-metal $3d$ orbitals can be measured by soft x-ray magnetic circular dichroism (XMCD) measurements of the $2p$ core level of the transition element¹⁷. Furthermore, in XMCD measurements, one can eliminate extrinsic magnetic signals such as those from oxidized Fe and those from the diamagnetic SiO₂ coating. In the present work, we have applied the XAS and XMCD techniques to the SiO₂-coated FePt nanoparticles to characterize their magnetic properties from the microscopic level.

FePt nanoparticle samples were prepared by the wet chemical method. Precursor fcc FePt nanoparticles were prepared according to the method of Sun *et al.*¹⁸, and were subsequently coated by SiO₂ according to the method of Fan *et al.*¹⁹. Thus during the heat treatment thermal diffusion of Fe and Pt atoms was confined inside the SiO₂ nanoreactor. For details of the fabrication process, we refer the reader to Yamamoto *et al.*⁹. For the XMCD measurements, the nanoparticle samples were supported by silver paste on a sample holder. After the preparation of the samples, they were kept in an Ar atmosphere in order to prevent oxidation until the XMCD measurements. XAS $[(\mu_+ + \mu_-)/2]$ and XMCD $(=\mu_+ - \mu_-)$ spectra were obtained at the helical undulator beam line BL23SU of SPring-8. Here, μ_+ and μ_- are XAS spectra taken with the light helicity parallel and antiparallel to the incident photon direction, respec-

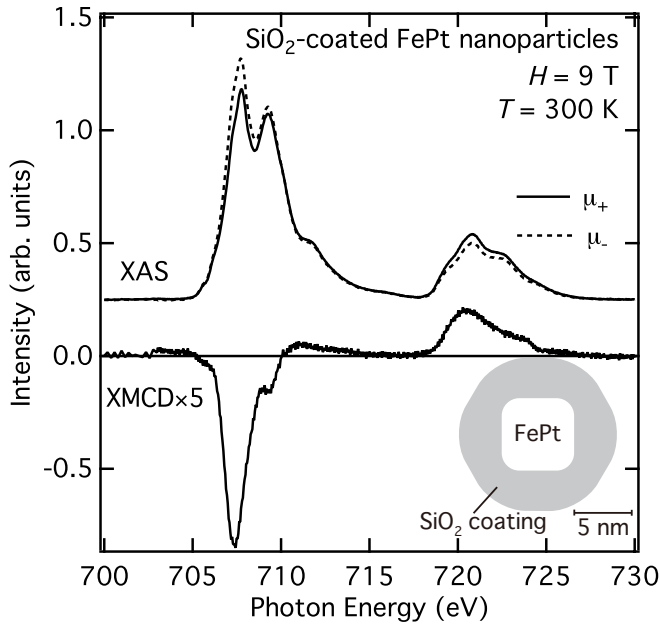


FIG. 1. (Color online) XAS and XMCD spectra at the Fe $L_{2,3}$ edges of the SiO_2 -coated FePt nanoparticles under the applied magnetic field of 9 T. All the spectra have been normalized to the L_3 XAS peak intensity. Inset shows a schematic figure of the FePt nanoparticle coated by SiO_2 . According to transmission electron microscopy (TEM) pictures reported by Yamamoto *et al.*⁹, the average size of the FePt nanoparticles is estimated to be 6-7 nm and that of the SiO_2 coat to be 10-15 nm.

tively. The highest applied magnetic field was 9 T. The measurements were done under an ultra-high vacuum of $\sim 4.8 \times 10^{-9}$ Pa. The polarity of the synchrotron radiation was switched at each photon energy using a kicker magnet with the frequency of 1 Hz²⁰. The measurements were done at room temperature (~ 300 K) in the total electron yield (TEY) mode. The magnetic field dependence of the XMCD intensity at the peak of the Fe L_3 edge was measured in the range of $-9 \text{ T} \leq H \leq 9 \text{ T}$.

Figure 1 shows the XAS and XMCD spectra at the Fe $L_{2,3}$ edges of the FePt nanoparticles. All the spectra have been normalized to the L_3 XAS peak intensity. Unlike the Fe $L_{2,3}$ spectra of FePt by Boyen *et al.*⁷ and Dmitrieva *et al.*⁸, each of the L_3 and L_2 edges exhibits a doublet structure: The L_3 doublet peaks are located at 707.7 eV and 709.3 eV, and the L_2 ones at 720.8 eV and 722.7 eV. Furthermore, broad shoulder/tail structures are observed on the high-energy side of the L_3 peak from 710 eV to 717 eV and on the high-energy side of the L_2 peak from 722 eV to 730 eV. We consider that the origin of the doublets is overlapping signals of FePt (at 707.7 and 720.8 eV) and Fe oxides (at 709.3 and 722.7 eV). The oxides are most likely extrinsic Fe^{3+} oxides formed at the surface of bare FePt particles whose SiO_2 -coating was removed when grinding the sample into fine powders, as one can see from the TEM picture [shown in Fig. 2(b) of

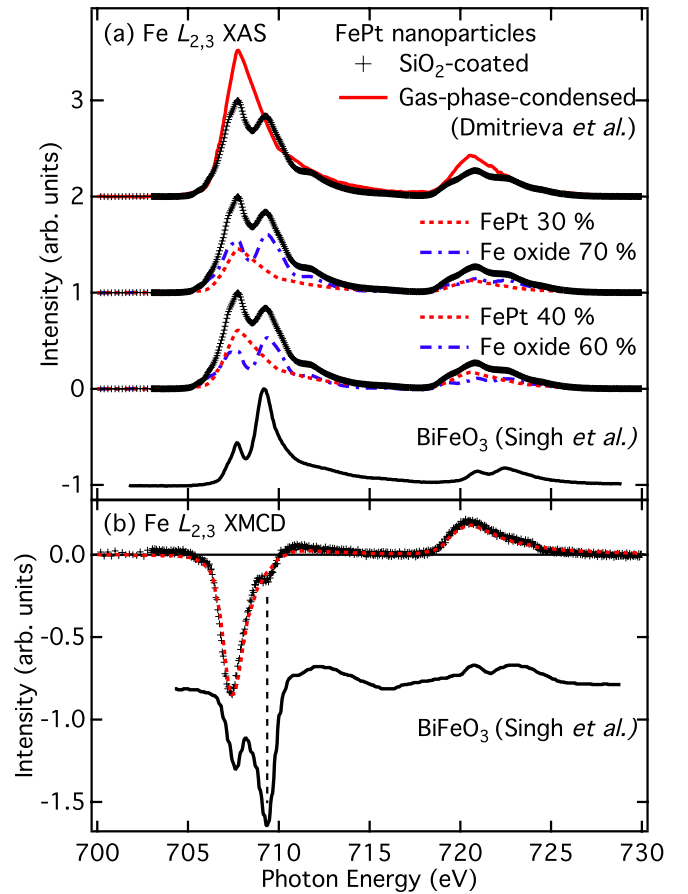


FIG. 2. (Color online) Decomposition of the measured XAS and XMCD spectra into those of FePt and a Fe^{3+} oxide. (a) The experimental XAS spectrum and that of gas-phase-condensed FePt nanoparticles (Ref. 8) are shown by crosses and a solid curve, respectively, at the top. Spectra after subtraction of the FePt ones (dotted curves) from the measured ones by different ratios are indicated below by dot-dashed curves. The XAS spectrum of BiFeO_3 by Singh *et al.*²² is shown at the bottom. (b) The experimental XMCD spectrum (crosses) and the FePt one (Ref. 8, dotted curve) are shown at the top. The XMCD spectrum of BiFeO_3 by Singh *et al.*²² is shown at the bottom.

Yamamoto *et al.*⁹]. We tentatively attribute the shoulder/tail structures to the charge-transfer $2p^5d^6-2p^5d^7\bar{L}$ satellite of the Fe^{3+} oxide²¹ but the exact origin of the structure remains to be clarified. On the other hand, the lineshape of the experimental XMCD spectrum in Fig. 1 is almost identical to that of FePt by Dmitrieva *et al.*⁸ except for a small negative peak around 709 eV, indicating that contributions of the Fe oxides to the XMCD spectrum are small.

In order to estimate signals of the Fe oxides, we first subtracted the FePt XAS spectrum reported by Dmitrieva *et al.*⁸, where Fe oxide was completely removed by plasma treatment, from the experimental one. In Fig. 2(a), one can see that after having subtracted the FePt XAS spectrum multiplied by ~ 0.4 , the spectral lineshape

TABLE I. Values of spin (M_{spin}) and orbital (M_{orb}) magnetic moments (in units of μ_{B}/Fe) and the coercive field H_c (in units of T) for different FePt samples.

	M_{spin}	M_{orb}	$M_{\text{orb}}/M_{\text{spin}}$	H_c
Nanoparticle (present work)	1.4	0.12	0.08	1.8
Nanoparticle (gas phase) ⁸	2.21	0.19	0.09	0.038
FePt thin films ²⁴	0.5	0.025	0.05 \pm 0.01	0.1

became similar to that of BiFeO₃, where the Fe³⁺ ion is located at the O_h site²², shown in the bottom of Fig. 2(a). Thus the intrinsic signals from FePt are estimated to be 40 % of the total Fe $L_{2,3}$ XAS intensity. The experimental XMCD spectrum at the Fe $L_{2,3}$ edges of the FePt nanoparticles is shown in Fig. 2(b). The lineshape of the XMCD spectrum of FePt nanoparticles prepared by the gas condensation method by Dmitrieva *et al.*⁸ is also shown by a dotted curve. Unlike the XAS spectra, both XMCD data agree with each other except for the small negative peak around 709 eV in the present sample. From comparison of the present XMCD spectrum with the XMCD spectrum of BiFeO₃ shown at the bottom of Fig. 2(b), the small negative peak can be attributed to a peak of a Fe³⁺ oxide. After having removed the Fe-oxide contributions from the experimental XAS and XMCD spectra, we applied the XMCD sum rules^{17,23} and obtained the spin moment $M_{\text{spin}} = 1.4 \mu_{\text{B}}/\text{Fe}$, the orbital moment $M_{\text{orb}} = 0.12 \mu_{\text{B}}/\text{Fe}$, and their ratio $M_{\text{orb}}/M_{\text{spin}} = 0.08$. These values are summarized in Table I, and are compared with those of different kinds of FePt samples^{8,24}. The obtained $M_{\text{orb}}/M_{\text{spin}}$ ratio is comparable to the value (0.09) obtained for FePt nanoparticles prepared by gas phase condensation⁸, and is larger than the values (~ 0.05) obtained for FePt thin films²⁴, indicating a high degree of $L1_0$ order. The deduced $M_{\text{spin}} = 1.4 \mu_{\text{B}}/\text{Fe}$ is, however, small compared to the other FePt samples ($\geq 2 \mu_{\text{B}}/\text{Fe}$). The origin of this discrepancy is not clear at present, but the outermost layers of the bare FePt particles might also be oxidized to Fe²⁺ and become non-ferromagnetic because the XAS and XMCD lineshapes of Fe²⁺ oxides and metallic Fe are hardly distinguishable.

Figure 3(a) shows the Fe L_3 -edge XMCD intensities of the FePt nanoparticles as functions of magnetic field at two different photon energies. The curve at $h\nu = 709.2$ eV, which reflects the XMCD signal of the Fe³⁺ oxide, is linear in H and shows no hysteretic behavior. Since the slope is given by the magnetic susceptibility χ of the Fe³⁺ ion of the oxide, it is given by C/T if the Fe³⁺ ion is paramagnetic or by C/T_N if it is antiferromagnetic. Here, C and T_N are the Curie constant for the Fe³⁺ ($S = 5/2$) ion and the Neel temperature, respectively. From the slope $\chi \sim 0.023 \mu_{\text{B}}/\text{T}$, we estimated T or $T_N \sim C/\chi = 325$ K, indicating that the Fe³⁺ at 300 K are paramagnetic or slightly below T_N , and cannot be ferro/ferrimagnetic.

In contrast, the XMCD intensity at $h\nu = 707.7$ eV, which is dominated by FePt, shows a hysteretic behavior with H_c of 1.8 T. Because a M - H curve of the peak

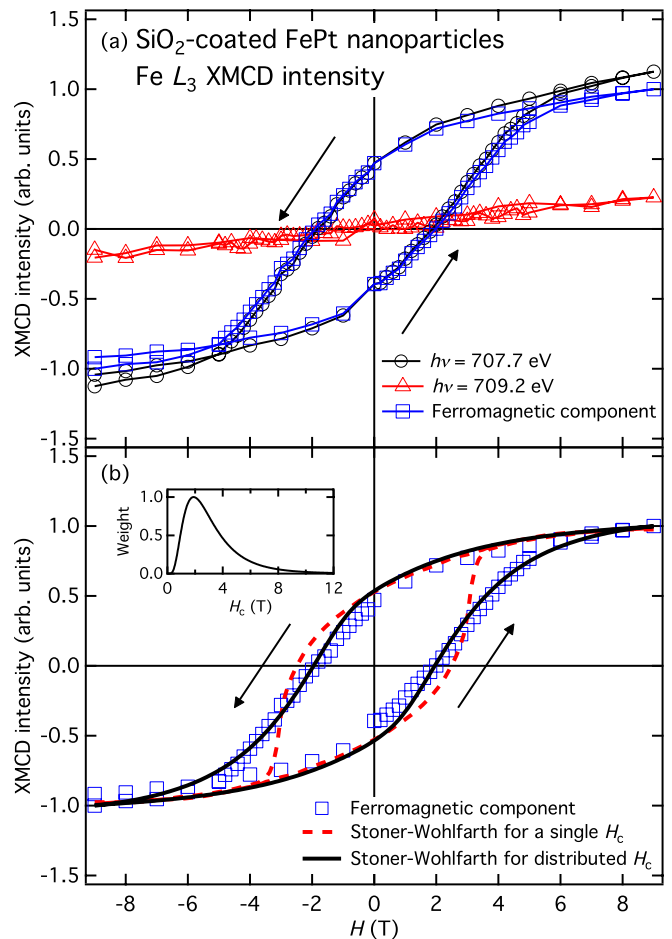


FIG. 3. (Color online) Hysteresis loops of the XMCD intensities (normalized to the saturation magnetization) at the Fe L_3 edge of the SiO₂-coated FePt nanoparticles. (a) Hysteresis loops at $h\nu = 707.7$ eV (open circles) and 709.2 eV (open triangles) corresponding to a peak due to FePt and the Fe³⁺ oxides, respectively. A ferromagnetic component extracted from the hysteresis loop at $h\nu = 707.7$ eV (open squares) is also plotted. (b) The ferromagnetic component of the XMCD hysteresis curve compared with a calculated Stoner-Wohlfarth hysteresis loop²⁵ for a single H_c ($= 2.5$ T) (dashed curve) and for distributed H_c (solid curve). Inset shows the log-normal distribution of H_c .

of the Fe oxides overlaps with the curve at $h\nu = 707.7$ eV, we obtained a M - H curve of a ferromagnetic component by subtracting the curve at $h\nu = 709.2$ eV from the curve at $h\nu = 707.7$ eV. From the shape of the hysteresis loop thus obtained as shown in Fig. 3(a), one can see that the value of the remnant magnetization is half of that of the saturation magnetization and the shape itself is somewhat rounded compared to a typical rectangular hysteresis loop for ferromagnetic materials. These behaviors are characteristic of the hysteresis of the Stoner-Wohlfarth model^{25,26}, which explains H_c based on the coherent reversal in non-interacting single-domain particles and in good agreement with some reports of nanoparti-

cle magnetism^{27,28}. Therefore, we first introduced the Stoner-Wohlfarth model with a fixed H_c ($= 2.5$ T) to reproduce the measured hysteresis loop, however, could not obtain a good fit as shown by a dashed curve in Fig. 3(b), because the experimental curve was broader in the high-field region. Then we assumed a distribution of H_c over a finite range (we assumed the log-normal distribution) as shown in the inset of Fig. 3(b). The calculated hysteresis loop shown in Fig. 3(b) reproduces almost all the characteristics of the experimental curve, indicating that the SiO₂-coated FePt nanoparticles act as non-interacting single-domain particles whose H_c is distributed from ~ 1 T to ~ 5 T. The distribution of H_c is possibly attributed to the distribution of structural defects of the FePt nanoparticles even though high degree of crystallinity is expected to be realized in the SiO₂-coated FePt nanoparticles as discussed below. Furthermore, because the Stoner-Wohlfarth model predicts $H_c = 0.48H_{c(e)}$, where $H_{c(e)}$ is the H_c for the magnetic field applied along the easy magnetization axis²⁶, the $H_{c(e)}$ of the present FePt nanoparticle sample is estimated as large as 3.75 T. This value is comparable to that of 4 T for FePt particulate films²⁹ and larger than those of 2.2 T for FePt (001) dot arrays³⁰ and 0.75 T for the microfabricated FePt (001) dots¹⁶, indicating the large magnetocrystalline anisotropy of the SiO₂-coated FePt nanoparticles.

Finally, we discuss the origin of the observed large H_c value for the SiO₂-coated FePt nanoparticles. The maximum single-domain size R_{sd} is estimated as $R_{sd} \approx 9\sqrt{\frac{k_B T_C}{2a_0} K_{1c}/\mu_0 M_s^2}$, where k_B , T_C , a_0 , K_{1c} , μ_0 , and M_s are the Boltzmann constant, Curie temperature, lattice constant, anisotropy constant, vacuum permeability, and saturation magnetization, respectively²⁵. Using typical values for FePt nanoparticles of $K_{1c} \sim 10^7$ erg/cc³¹, $a_0 = 0.386$ nm³² and $M_s = 2.4 \mu_B/\text{Fe}^8$, we estimate the lower limit of R_{sd} as ~ 100 nm, orders of magnitude larger than the particle size. Therefore, the SiO₂-coated FePt

nanoparticles can form in single domains and hence obtain the large H_c . If defects are present in the nanoparticles, they hinder the single-domain formation because the defects act as nucleation centers¹⁶. Thus, nucleation sites would lead to an enhancement of the H_c . In our fabrication method, the SiO₂ coating protects the small enough FePt nanoparticle from extra dispersion, deterioration, and oxidization during the sample preparation, leading to isolated single-domain FePt particles, and eventually to the large H_c value.

In conclusion, we have investigated the spin and orbital magnetic moments of Fe in FePt nanoparticles coated with SiO₂ using XMCD measurements. The deduced ratio of the orbital to spin magnetic moments $M_{orb}/M_{spin} = 0.08$ is nearly equal to that of FePt nanoparticles (0.09) condensed from gas phase for which oxidized layers were removed by *in situ* plasmas treatment⁸. The magnetization measured by Fe L_3 -edge XMCD was saturated around 6 T and H_c was as large as 1.8 T, much larger than the H_c (~ 0.038 T) of the gas phase condensed samples⁸, and consistent with the result of the SQUID measurement¹². The XMCD intensity versus magnetic field curve was fitted to the Stoner-Wohlfarth model for non-interacting single-domain nanoparticles whose H_c is distributed between ~ 1 T to ~ 5 T.

This work was supported by a Grant-in-Aid for Scientific Research from the JSPS (S22224005) and the ‘‘Quantum Beam Technology Development Program’’ of JST. The experiment was done under the approval of the Photon Factory Program Advisory Committee (proposal No. 2010G187), under the Shared Use Program of JAEA Facilities (Proposal No. 2011A3840), and at JAEA beamline in SPring-8 (proposal No. 2011B3823 and 2012A3823/BL23-SU). SY acknowledges financial support from MEXT KAKENHI (20104006). YT was supported by JSPS through the Program for Leading Graduate Schools (MERIT).

* takahashi@wyvern.phys.s.u-tokyo.ac.jp

¹ O. A. Ivanov, L. V. Solina, V. A. Demshina, and L. M. Magat, Phys. Met. Metallogr. **35**, 81 (1973).

² S. Okamoto, N. Kikuchi, O. Kitakami, T. Miyazaki, Y. Shimada, and K. Fukamichi, Phys. Rev. B **66**, 024413 (2002).

³ T. Seki, S. Mitani, K. Yakushiji, and K. Takanashi, Appl. Phys. Lett. **88**, 172504 (2006).

⁴ T. Seki, S. Mitani, and K. Takanashi, Phys. Rev. B **77**, 214414 (2008).

⁵ O. Dmitrieva, M. Acet, G. Dumpich, J. Kästner, C. Antoniak, M. Farle, and K. Fauth, J. Phys. D: Appl. Phys. **39**, 4741 (2006).

⁶ S. Yamamoto, Y. Morimoto, Y. Tamada, Y. K. Takahashi, K. Hono, T. Ono, and M. Takano, Chem. Mater. **18**, 5385 (2006).

⁷ H.-G. Boyen, K. Fauth, B. Stahl, P. Ziemann, G. Kästle,

F. Weigl, F. Banhart, M. Hessler, G. Schütz, N. Gajbhiye, J. Ellrich, H. Hahn, M. Büttner, M. Garnier, and P. Oelhafen, Adv. Mater. **17**, 574 (2005).

⁸ O. Dmitrieva, M. Spasova, C. Antoniak, M. Acet, G. Dumpich, J. Kästner, M. Farle, K. Fauth, U. Wiedwald, H.-G. Boyen, and P. Ziemann, Phys. Rev. B **76**, 064414 (2007).

⁹ S. Yamamoto, Y. Morimoto, T. Ono, and M. Takano, Appl. Phys. Lett. **87**, 032503 (2005).

¹⁰ Y. Morimoto, T. Tamada, S. Yamamoto, T. Ono, and M. Takano, J. Magn. Soc. Jpn. **40**, 464 (2006).

¹¹ Y. Tamada, Y. Morimoto, S. Yamamoto, N. Hayashi, M. Takano, S. Nasu, and T. Ono, Jpn. J. Appl. Phys. **45**, L1232 (2006).

¹² Y. Tamada, S. Yamamoto, M. Takano, S. Nasu, and T. Ono, Appl. Phys. Lett. **90**, 162509 (2007).

¹³ Y. Tamada, Y. Morimoto, S. Yamamoto, M. Takano,

- S. Nasu, and T. Ono, *J. Magn. Magn. Mater.* **310**, 2381 (2007).
- ¹⁴ D. Wang, T. Seki, K. Takanashi, T. Shima, G. Li, H. Saito, and S. Ishio, *J. Appl. Phys.* **105**, 07A702 (2009).
- ¹⁵ Y. Tanaka, N. Kimura, K. Hono, K. Yasuda, and T. Sakurai, *J. Magn. Magn. Mater.* **170**, 289 (1997).
- ¹⁶ D. Wang, T. Seki, K. Takanashi, and T. Shima, *J. Phys. D: Appl. Phys.* **41**, 195008 (2008).
- ¹⁷ B. T. Thole, P. Carra, F. Sette, and G. van der Laan, *Phys. Rev. Lett.* **68**, 1943 (1992).
- ¹⁸ S. Sun, C. B. Murray, D. Weller, L. Folks, and A. Moser, *Science* **287**, 1989 (2000).
- ¹⁹ H. Fan, K. Yang, D. M. Boye, T. Sigmon, K. J. Malloy, H. Xu, G. P. López, and C. J. Brinker, *Science* **304**, 567 (2004).
- ²⁰ Y. Saitoh, Y. Fukuda, Y. Takeda, H. Yamagami, S. Takahashi, Y. Asano, T. Hara, K. Shirasawa, M. Takeuchi, T. Tanaka, and H. Kitamura, *J. Sync. Rad.* **19**, 388 (2012).
- ²¹ J. P. Crocombette, M. Pollak, F. Jollet, N. Thromat, and M. Gautier-Soyer, *Phys. Rev. B* **52**, 3143 (1995).
- ²² V. R. Singh, V. K. Verma, K. Ishigami, G. Shibata, Y. Yamazaki, A. Fujimori, Y. Takeda, T. Okane, Y. Saitoh, H. Yamagami, Y. Nakamura, M. Azuma, and Y. Shimakawa, *J. Appl. Phys.* **114**, 103905 (2013).
- ²³ P. Carra, B. T. Thole, M. Altarelli, and X. Wang, *Phys. Rev. Lett.* **70**, 694 (1993).
- ²⁴ S. Imada, A. Yamasaki, S. Suga, T. Shima, and K. Takanashi, *Appl. Phys. Lett.* **90**, 132507 (2007).
- ²⁵ J. M. D. Coey, *Magnetism and Magnetic Materials* (Cambridge University Press, 2010).
- ²⁶ E. C. Stoner and E. P. Wohlfarth, *Phil. Trans. R. Soc. A* **240**, 599 (1948).
- ²⁷ M. Chuev, *J. Exp. Theor. Phys. Lett.* **85**, 611 (2007).
- ²⁸ L.-M. Lacroix, R. B. Malaki, J. Carrey, S. Lachaize, M. Respaud, G. F. Goya, and B. Chaudret, *J. Appl. Phys.* **105**, 023911 (2009).
- ²⁹ T. Shima, K. Takanashi, Y. K. Takahashi, and K. Hono, *Appl. Phys. Lett.* **81**, 1050 (2002).
- ³⁰ T. Seki, T. Shima, K. Yakushiji, K. Takanashi, G. Q. Li, and S. Ishio, *J. Appl. Phys.* **100**, 043915 (2006).
- ³¹ N. A. Usov and J. M. Barandiaran, *Appl. Phys. Lett.* **101**, 172402 (2012).
- ³² T. J. Klemmer, N. Shukla, C. Liu, X. W. Wu, E. B. Svedberg, O. Mryasov, R. W. Chantrell, D. Weller, M. Tanase, and D. E. Laughlin, *Appl. Phys. Lett.* **81**, 2220 (2002).